8-1-2022

Investigating the Acoustic Properties of Polymer Microspheres Suspended in Gelatin

Alexander Orlin Denette

Recommended Citation

Denette, Alexander Orlin, "Investigating the Acoustic Properties of Polymer Microspheres Suspended in Gelatin" (2022). *Electronic Theses and Dissertations*. 2367.
https://egrove.olemiss.edu/etd/2367

INVESTIGATING THE ACOUSTIC PROPERTIES OF POLYMER MICROSPHERES SUSPENDED IN GELATIN

A Thesis
presented in partial fulfillment of the requirements
for the degree of Master of Science
in the Department of Physics and Astronomy
The University of Mississippi

by
ALEXANDER ORLIN DENETTE
Aug 2022

Abstract

Recent advancements in materials science have produced materials that exhibit properties with values outside of naturally observed ranges. These properties are driven by overlapping, low order resonant modes, and are limited to small response ranges close to harmonic frequencies. This study aims to see if the same properties can be recreated with high order resonant modes from distributions of small scatterers. A method for holding random distributions of scatterers in space was created, and two types of acoustic measurements were taken. Resonant frequencies and their scattering order were identified, and the resulting scattered fields were resolved.

Dedication

I would like to dedicate this work to my late cat, Mr. Buckles.

Symbols Used

$F(\omega)$ is a harmonically driven force,

$\overline{M}(\omega)$ is the effective mass of the system

$\frac{d^2x}{dt^2}$ is the acceleration

ω_o is the resonant frequency

ω is the driving frequency

c is the speed of sound

x is the thickness of the sample

$\overline{P_i}$ is the incoming wave

$\overline{P_o}$ is the maximal amplitude of the wave

n is the order of the mode

$j_n(kr)$ is the Spherical Bessel Function of the n^{th} order

$P_n(\cos(\theta))$ is the Legendre polynomial of n^{th} order

$\overline{P_s}$ is the scattered wave

$h_n^1(kr)$ is the outgoing Henckel Function of the n^{th} order

k is the wave vector

$q(t)$ is the waveform recorded from a sample

$f(t')$ is the impulse from the incoming ultrasound

$p(t - t')$ is the natural transfer function of the scatterers

$Q(\omega)$ is the recorded sample spectrum

$W(\omega)$ is the spectrum of the water path data

$P(\omega)$ is the spectrum of the transfer function

α is the attenuation

Acknowledgements

I would like to thank Dr. Cecille Labuda for her unwavering support of my goals at the University of Mississippi. There have been several points on this journey where it felt impossible, but she was always there to give advice or recommendations to help me stay on the path. From undergraduate lectures to thesis advisor, she has truly been an inspiration, and one of the most important figures in my educational experience.

I would also like to thank Dr. Joel Mobley for agreeing to let me work with the Ultrasonics group, and for sitting on my defense committee. His insight and knowledge have been another constant during my time at the University of Mississippi. As the professor of the first physics course I took here, it was particularly fitting to have him close my career here as well.

Furthermore, I would like to thank Dr. Luca Bombelli, the final member of my defense committee and the chair of the department. Dr. Bombelli has shown me kindness and patience in the face of many failures and adversities, and without that continued support, I would not have been able to accomplish this dream.

Table of Contents

List of Tables

List of Figures

Chapter I: Introduction

Section 1.1: Background

Acoustic waves are mechanical waves that span a wide range of frequencies, as can be seen in Figure 1.1 where the acoustic spectrum is illustrated. Acoustic vibrations within the audible range are colloquially referred to as sound, while acoustic waves above and below this range are referred to as ultrasound and infrasound respectively.

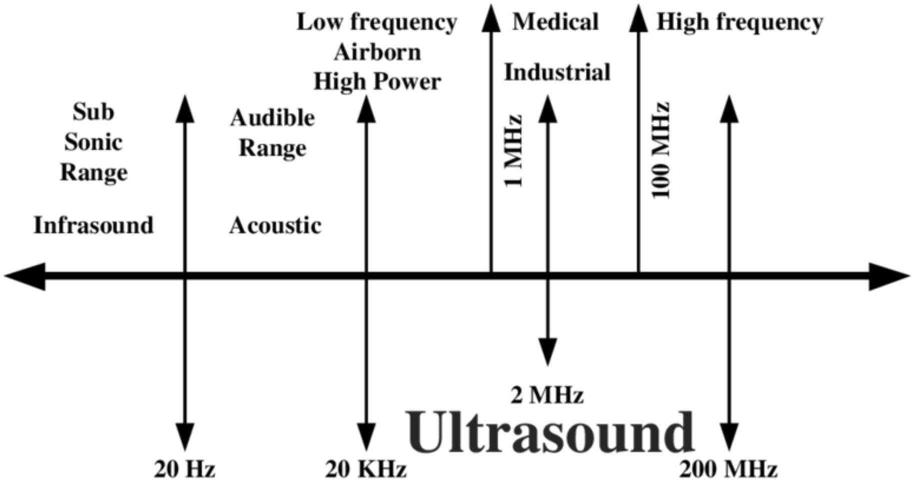

Figure 1.1: The acoustic spectrum. The three divisions of the spectrum have been labeled, along with subdivisions specific to other frequencies [1].

In this study, the effect of a compact distribution of polyethylene microsphere scatterers on a propagating ultrasound beam was investigated. The wavelength of the ultrasound was of the same order of magnitude as the size of the microspheres, allowing the excitation of their resonant scattering modes. It has been shown that for mechanical systems, regular motion close to the resonant frequencies can produce negatively valued material properties, such as mass density [2]. Currently, materials that support these properties have narrow response ranges, due to their reliance upon excitations near resonant frequencies. An example of how harmonically driven motion can result in a negative physical parameter is easiest to create in one dimension. The explicit effect of frequency on the mass of the system is seen with Equation 1.1.

$$F(\omega) = \overline{M}(\omega)\frac{d^2x}{dt^2} \qquad (1.1.a)$$

$$\overline{M}(\omega) = M_1 + \frac{K}{\omega_o - \omega}M_2 \qquad (1.1.b)$$

Eq. 1.1 is equation of motion for a system that supports negative mass, $F(\omega)$ is a harmonically driven force, $\overline{M}(\omega)$ is the effective mass of the system, and $\frac{d^2x}{dt^2}$ is the acceleration of the mass. The effective mass is the mass of the overall cavity plus a perturbation due to the oscillation of the interior. ω_o is the resonant frequency of the spring system, and ω is the driving frequency of the force. The difference between the driving frequency and the resonant frequency can take on a range of small, negative values, which can cause the overall mass to become effectively negative. In Figure 1.2, a rendering of masses and a spring coupled in a frictionless interior is shown. This model corresponds to the situation described by Eq. 1.1

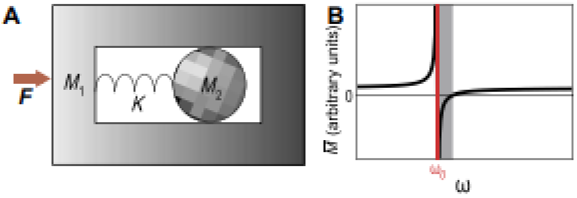

Figure 1.2: a) A mass, M_2, is attached to the frictionless interior of M_1 by a spring with mass K. A force, F, is applied to M_1 from the left side periodically. b) Effective mass of M_1 as the driving frequency ω increases. When $\omega=\omega_o$, the resonant frequency of the interior spring system, the effective mass is negative for a small range of ω that is highlighted [3].

Negative properties generally exhibit this behavior, but only at frequencies close to the resonant frequencies of material. These negative properties produced by the resonant frequencies depend on the symmetry of the resonant mode however. Resonant modes of odd order produce changes to the center of mass, leading to negative mass. The even order modes produce changes in the shape of the scatterer and lead to negative bulk modulus. To achieve a doubly negative material, both monopolar and dipolar behavior must occur at the same frequency [3-5]. It is hypothesized that the same negative parameters could be potentially seen when higher order even and odd resonant modes are mixed, providing a broader working range for acoustic metamaterials, materials that have been engineered to have specific parameters. Work with scattering from microspheres has shown that they exhibit a range of resonant frequencies that can be excited using readily available transducers [5-8]. Furthermore, microsphere scatterers behave ideally, and acoustic measurements of their properties agree well with theoretical predictions, seen in Figure 1.3 on the next page. Potentially, negative parameters of acoustic metamaterials can be engineered to respond at several frequencies by choosing the right combination of microsphere scatterers with overlapping even and odd scattering modes. In this work, the results of an investigation of how different size ranges of microspheres responded to broadband ultrasonic signals ranging 1 – 35 MHz are presented, taking particular interest in the overlap between even and odd resonant frequencies.

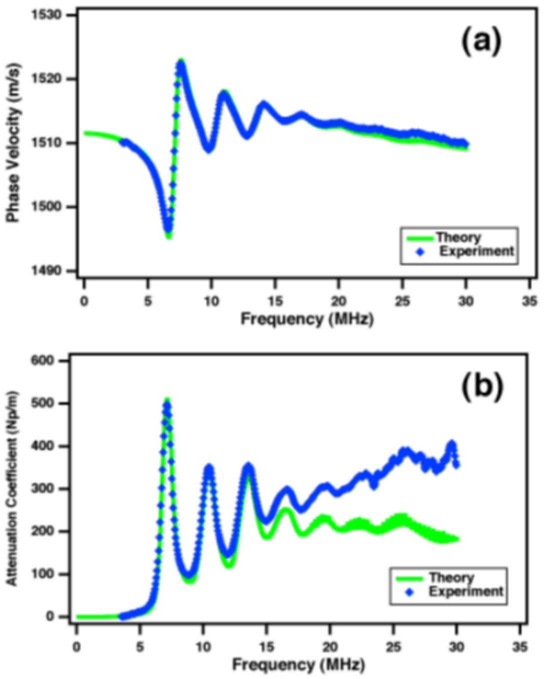

Figure 1.3: a) theoretical and experimental measurements of phase velocity for r = 50 µm microspheres. b) theoretical and experimental measurements of attenuation for r = 50 µm microspheres [6].

Section 1.2: Metamaterials

Metamaterials are engineered materials that have specific properties that typically do not exist in homogeneous materials. A type of metamaterial of great interest is known as a double negative material. These materials have been created such that two of their key material parameters can simultaneously be negatively valued, when naturally they would be positive. While these materials are often used for their unique electronic properties, mechanical metamaterials have become a popular research area in recent years [2-5]. By taking advantage of resonant properties, materials can be engineered that will exhibit negative mass and bulk modulus when excited at frequencies close to the monopolar and dipolar resonant frequencies. Acoustic metamaterials are the end goal for this research, as they can be used in a variety of situations such as lensing and waveguides, providing ways to focus diverging beams or guiding acoustic waves either towards or away from an object of interest [3].

Section 1.3: Resonance and Scattering

Spherical waves are generally modeled using Equation 1.2.

$$\overline{P_i} = \overline{P_o} \sum_{n=0}^{\infty} (2n + 1) i^n j_n(kr) P_n(\cos(\theta)) \qquad (1.2)$$

$\overline{P_i}$ is the incoming wave, n is the order of the mode, $\overline{P_o}$ is the maximal amplitude of the wave, $j_n(kr)$ is the Spherical Bessel Function of the n^{th} order, and $P_n(\cos(\theta))$ is the Legendre polynomial of n^{th} order [9]. When waves interact with an object, they impart some of their energy to deform the object and that energy is transmitted as a scattered wave. When the object's size is the same order of magnitude as the wavelength, a specific phenomenon known as resonance may occur. When resonance occurs, a spherical object exposed to an incoming wave will deform in shapes governed by Legendre polynomials. The object will radiate a scattered acoustic wave at the same frequency, called the resonant frequency, as the exciting wave. This scattered wave can be modeled using Equation 1.3.

$$\overline{P_s} = \overline{P_o} \sum_{n=0}^{\infty} c_n (2n + 1) i^n h_n^1(kr) P_n(\cos(\theta)) \qquad (1.3)$$

$\overline{P_s}$ is the scattered wave, n is the order of the mode, $\overline{P_o}$ is the maximal amplitude of the wave, $h_n^1(kr)$ is the outgoing Henckel Function of the n^{th} order, and $P_n(\cos(\theta))$ is the Legendre polynomial of n^{th} order [9]. When dealing with a distributed collection of similarly sized scatterers, the average scattered field can reflect the individual resonant frequencies of the group. Therefore, one can observe the physical characteristics of the individual objects based on their aggregate behavior. Previous studies have demonstrated where scattering modes should occur relative to wavelength and circumference of the scatters [6]. This is seen in figure 1.4.

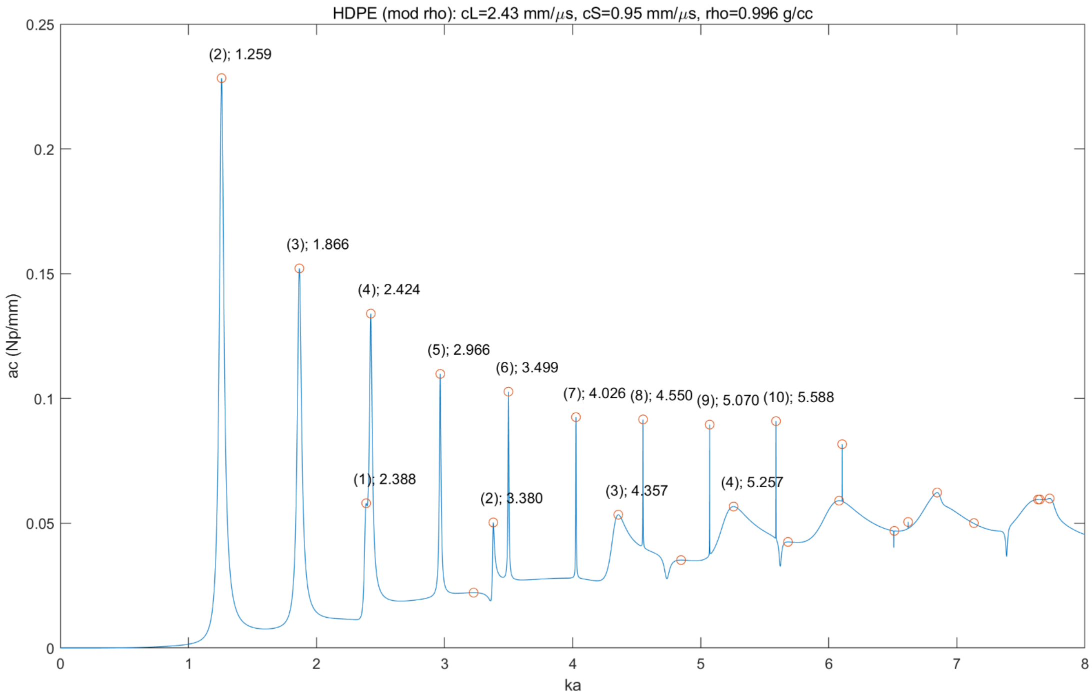

Figure 1.4: Scattering order relative to ka, the product of the wave vector and the circumference of the scatter.

Chapter II: Methods

Section 2.1: Sample Specifications and Production

The scattering samples in this study were prepared using a gelatin solution infused with polyethylene microspheres acquired from Cospheric (3622 Capri Drive Santa Barbara, California 93160 United States). Three sizes of spheres were used in this study, listed in increasing radius: orange polyethylene spheres (r = 98 μm), and purple polyethylene spheres (r = 116 μm), and red polyethylene spheres (r = 138 μm). Physical properties of the samples can be found in Table 2.1.

Color	Size Range (μm)	Average Radius (μm)	Density (g/cm^3)	Number density
Orange	180-212	98	1.00	2.54×10^5
Purple	212-250	116	1.00	1.55×10^5
Red	250-300	138	0.98	9.18×10^4

Table 2.1: Physical properties of the various samples used in this study. The color served as a visual indicator of scatterering type. The reported size range refers to the diameter of the spheres.The spheres per gram column represents an average value for the size range given.

The samples were created by using a mold in which a mixture of gelatin solution and scatterers was allowed to set. The molds are made from cross sections of a plexiglass tube, with internal volumes of 12.8 ml per mold and a thickness 1.3 cm. The plexiglass rings served as the walls of the mold, and the base was created by affixing the walls to a flat sheet of plexiglass using high vacuum grease. A picture of one of the molds can be found in Fig. 2.1.

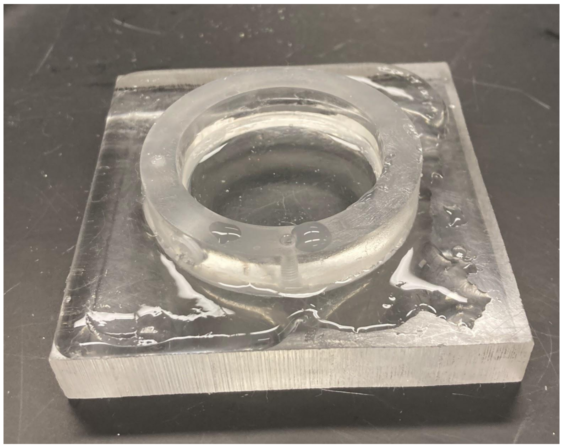

Fig. 2.1: A mold loaded with a blank gelatin solution.

The gel formula reported in Table 2.2 produces enough gelatin solution for two molds, or roughly 25.6 ml of solution.

Reagent	Volume (ml)	Weight (g)
Gelatin		1.24
Distilled Water	20	
Formaldehyde	3.2	
1-Propanol	1.4	
Microspheres		Varies (see Table 2.3)

Table2.2: List of reagents and their quantities for the production of two samples. The liquid components total 24.6 ml and the gelatin has a density in the range of 1.3-1.4 g/ml, producing a final solution volume in slight excess of 25.6 ml.

Samples were designed to hold random distributions of microspheres in a material that is acoustically transparent, to minimize interference in the scattered signal due to the matrix. Production requires precision and speed to make usable samples. While the microspheres were advertised as being neutrally buoyant, there was some discrepancy between the density of the spheres and the gelatin solution. The density of the solution was greater than that of pure water due to the addition of alcohol (necessary to stiffen the gelatin matrix to prevent lowering the speed of sound), formaldehyde (necessary to catalyze the gelatin crosslinking in the setting process), and gelatin. This discrepancy caused a net migration of the microspheres to the top of the solution as it was setting, causing large local concentrations of scatterers near one surface of the set sample. Regular mechanical agitation can be used to maintain the random distribution, maintaining a relatively even scatterer concentration through the sample. However, at a certain point in the setting process (roughly 5 minutes), mechanical agitation can disrupt the gelatin cross links and produce local areas of high microsphere concentration, potentially fully attenuating portions of the ultrasound beam. Methods of sample production involving completely sealing the mold were tested as well, but issues with air bubble inclusions prevented these methods from being useful. Microsphere concentrations were determined through trial and error, with initial scatterer concentrations (almost 150,000 spheres per ml or s/ml) fully attenuating the ultrasonic beam. The upper limit of scatterer concentration was not empirically determined but signal transmission was seen at concentrations as high as 3.0 ks/ml, where ks/ml is the unit for 1000 s/ml. The lower limit of scatterer concentration was limited by the equipment used in production. The electronic balance used had an uncertainty of 0.001 g, or roughly 250 spheres. It was observed that concentrations of 1.0 ks/ml offered the best balance between material cost, ease of sample production, and signal response. Storage methods provided unique areas for sample failure. Samples stored fully submerged in water experienced significant swelling due to positive osmotic pressure pushing water into the gelatin matrix, altering effective scatterer concentration. Ideal storage conditions involved keeping the samples in small amounts of water in covered petri dishes such that the samples were only partially submerged and evaporation was inhibited. This method keeps osmotic pressure close to zero, preventing sample swelling and deformation. For production, the gelatin and microspheres were weighed separately in weigh-boats, and the distilled water, formaldehyde and 1-propanol were measured in 100 ml, 10 ml, and 5ml graduated cylinders, respectively. The distilled water was heated to 30 °C in a water bath, at which point the 1-propanol and gelatin were added. The solution was then stirred vigorously and allowed to heat up to 50 °C. The gelatin solution was removed from heat and stirred until all gelatin was dissolved, requiring occasional heating to maintain the 50 °C temperature. The fully dissolved solution was then placed in an ice water bath allowing the temperature to steadily fall to 30 °C without inducing gelatin setting. The formaldehyde was added just before pouring the solution. The microspheres may be introduced at several points depending on the type of samples being created. For multiple samples of the same concentration, the microspheres were added after the solution is raised to 50°C. Allowing the microspheres to reach thermal equilibrium with the solution prevents the gelatin solution from setting unevenly. For multiple samples of different concentrations, the spheres were weighed and then placed in the molds before the solution was poured. This method requires extra care, as the formaldehyde needs to be poured into the molds first to facilitate the mixing process. The solution was immediately agitated after pouring, creating the random arrangement of microspheres necessary for this study. Trace amounts of a strong detergent were added to prevent electrostatic clumping of the microspheres within the solution. The poured solution was cooled on the lab bench for 5-8 minutes, with periodic agitation every 2 minutes to keep the distribution random. After the gelatin solution was set enough to prevent microsphere migration due to density variation, the molds were placed in a freezer for another 10-15 minutes to fully set. A selection of samples with their scatterer concentrations can be found in Table 2.3.

Mean scatterer radius	Added mass (g)
r = 98 µm	0.050
r = 116 µm	0.080
r = 138 µm	0.139
Mixed, *r* = 98 µm & *r* = 116 µm	0.028 (*r* = 98 µm) 0.039 (*r* = 116 µm)

Table 2.3: Sample types are separated by scatterer radius. The total concentration of each sample was 1.0 ks/ml.

Pictures of some of the samples can be seen in Figure 2.2.

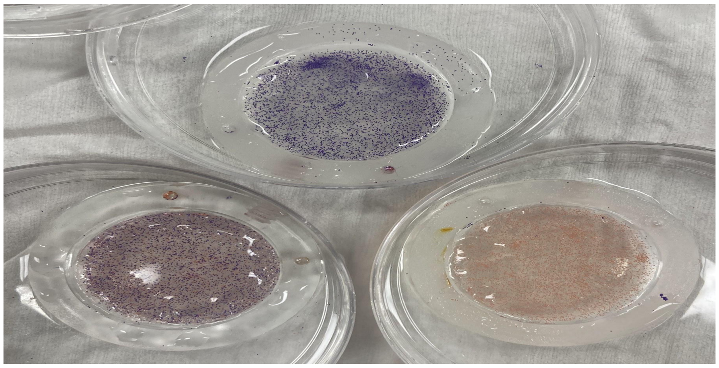

Figure 2.2: The top sample is the *r* = 116 µm sample, the bottom left is the (*r* = 98 µm) + (*r* = 116 µm) mixed sample and the bottom right is the *r* = 98 µm sample.

Section 2.2: Experimental Design

The samples were analyzed using two types of water tank based systems, both employing the through substitution method of analysis. The measurements were focused on two regions, one between 1-35 MHz for broadband measurements and the other between 1-15 MHz for the field measurements. Piezoelectric immersion transducers by pulser/receivers were used to create the necessary ultrasonic pulses. These transducers were impedance matched with water to maximize the amount of energy transmitted into the tank.

Section 2.2.1: The Measurement Tank

The initial setup used to determine the samples' properties is referred to as the measurement tank. The measurement tank was used to determine where the resonant frequencies are located in the spectrum for each sample type. The measurement tank is a 20 gallon tank made from plexiglass, with two linear, broadband transducers [Panametrics (221 Crescent Street Waltham, MA 02453 United States), Immersion P120-2] acting as the transmitter and receiver, connected to a pulser/receiver [Panametrics-NDT Model 5800] and an oscilloscope [Keysight (1400 Fountaingrove Parkway Santa Rosa, CA 95403) InfiniiVision DSOX2012A]. A schematic of the measurement tank can be seen in Figure 2.3.

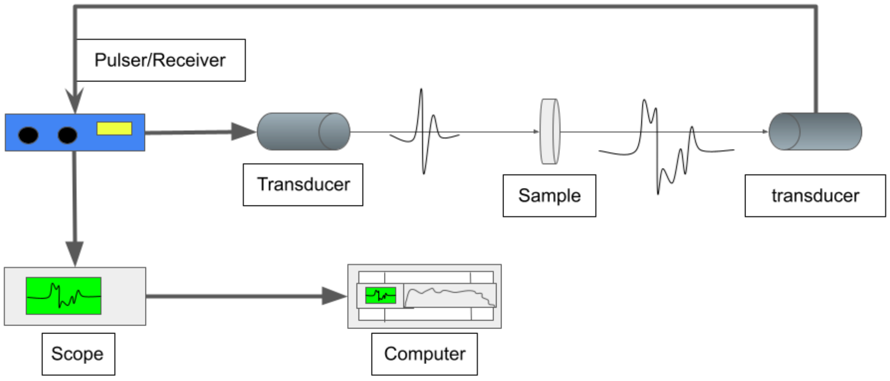

Figure 2.3: A basic schematic of the measurement tank

The transducers were attached to the tank using translating stages, such that adjustments could be made to the alignment along the 3 spatial axes and along the angle orthogonal to the mount. The measurement tank can be seen in Figure 2.4.

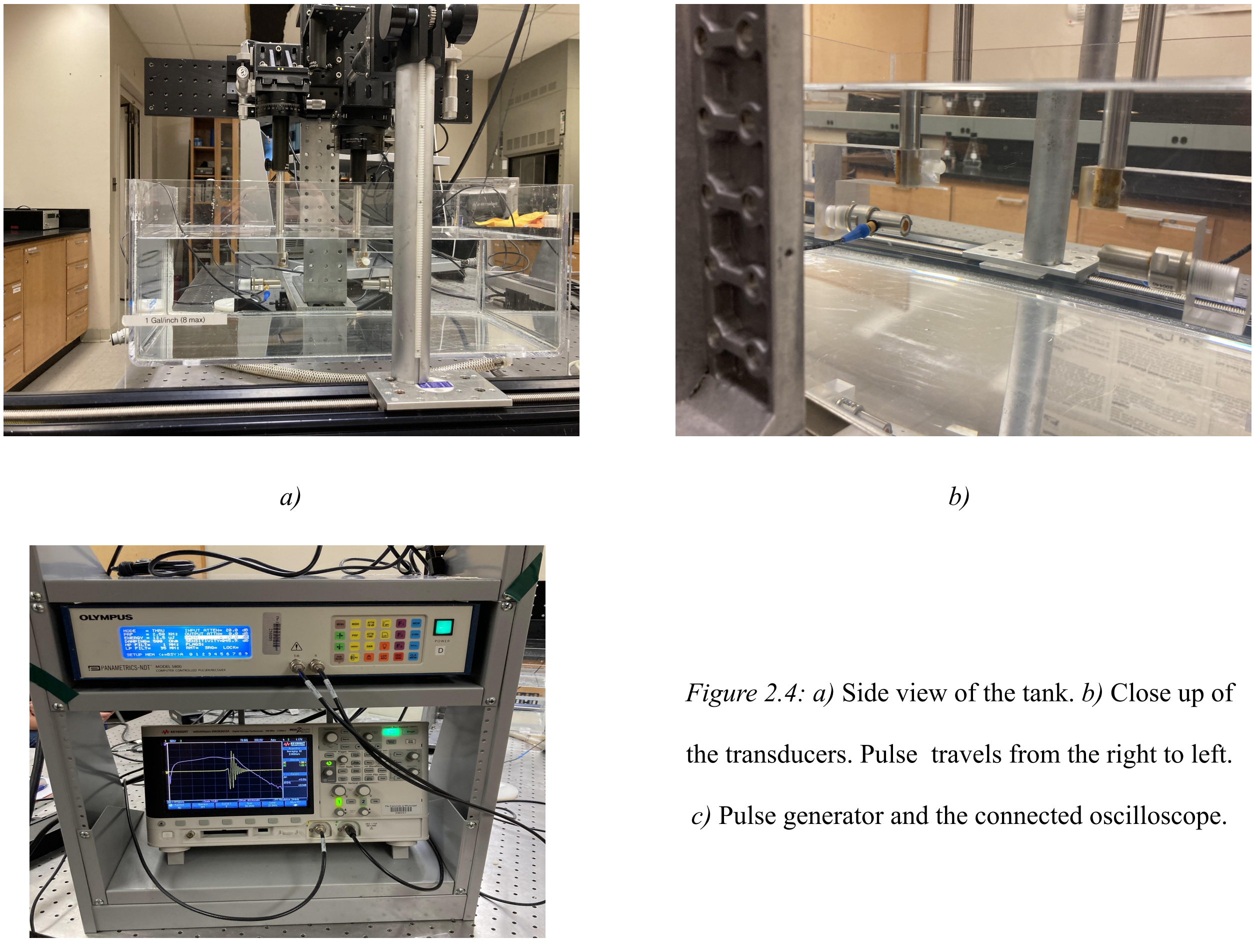

a)

b)

c)

Figure 2.4: a) Side view of the tank. *b)* Close up of the transducers. Pulse travels from the right to left. *c)* Pulse generator and the connected oscilloscope.

In this tank, samples were interrogated by broadband ultrasonic pulses which contain a broad spectrum of frequencies, spanning 1-35 MHz. This frequency range is limited for two reasons. The lower bound was set to filter out responses below the threshold of ultrasound, and the upper limit was set due to a lack of scatterer response to higher frequencies. The transducers used in this setup utilized a type of polymer for the element that allowed for broad acoustic response. The transducers were incredibly sensitive to changes in alignment due to the diffraction in the broadband beam. Furthermore, this tank was unable to resolve the angular field scattered from the sample, as this setup only records scattering along the forward direction. From the acoustic response of the samples, attenuation curves were produced that displayed the resonant frequencies of the scatterers. This analysis is discussed further in Chapter IV. The determined frequencies were used to guide the analysis of the 2D pressure field data, outlined further in the following sections.

Section 2.2.2: The Pressure Field Scanning Tank

The pressure field scanning tank was used to resolve the pressure amplitude of the field scattered from the samples over a defined area in 2 dimensions. By assigning points to the scan area, the waveform at each point is recorded and decomposed in a frequency spectrum by a process outlined in the following chapter. These spectra can be used to create frequency resolved images of the pressure distribution in the scan area. The pressure field scanning tank is a 50 gallon plexiglass tank. In this setup, a single transducer [Panametric NDT V309] is used as the transmitter and a needle hydrophone [Muller-Platte Needle Probe, (Hasengarten 35, 61440 Oberursel Germany)] as a receiver. They are connected to a pulser/receiver module [Panametric NDT Model 5072PR] used to create and record ultrasound pulses. The pulser/receiver was connected to an oscilloscope [Agilent 54622A, (5301 Stevens Creek Blvd, Santa Clara, CA 95051 United States] which is in turn connected to a computer serving as the control module. A schematic of this system can be seen in Figure 2.5

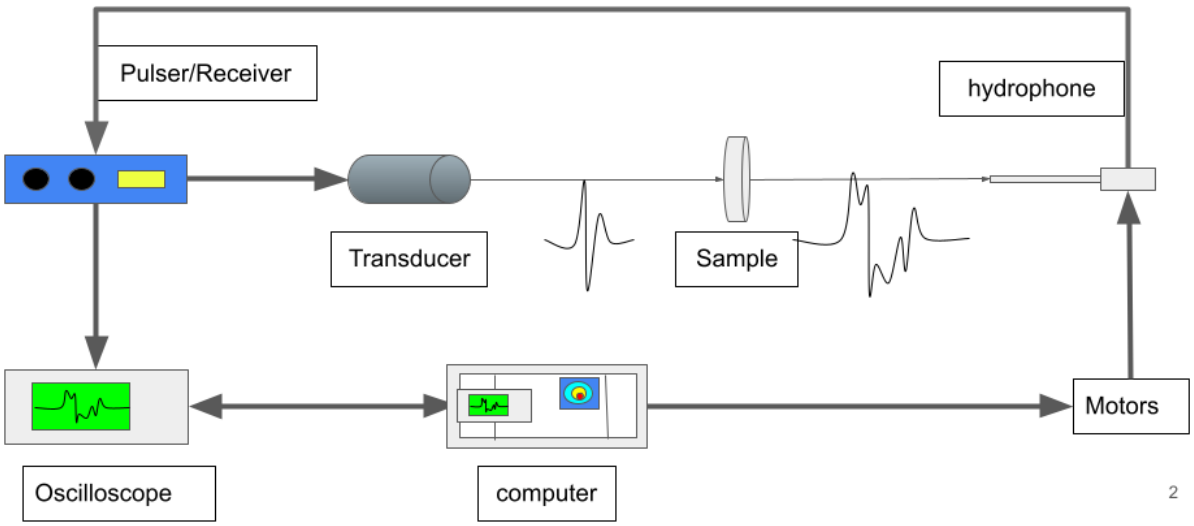

Figure 2.5: Basic schematic of the field scanning system.

The transducer is anchored to the tank, whereas the sample is placed in a rotary mount allowing control over the angle of incidence. This was kept as close to 90 degrees as possible, keeping the sample face parallel to the scanning plane. The hydrophone is able to move in three dimensions, using a Centroid Motion Controller motor system controlled by the computer. The probe's initial point was treated as the center of the scan region. Scans were limited to two dimensions in the plane perpendicular to the line made by the transducer, sample, and initial probe position. A picture of the tank can be seen in Figure 2.6

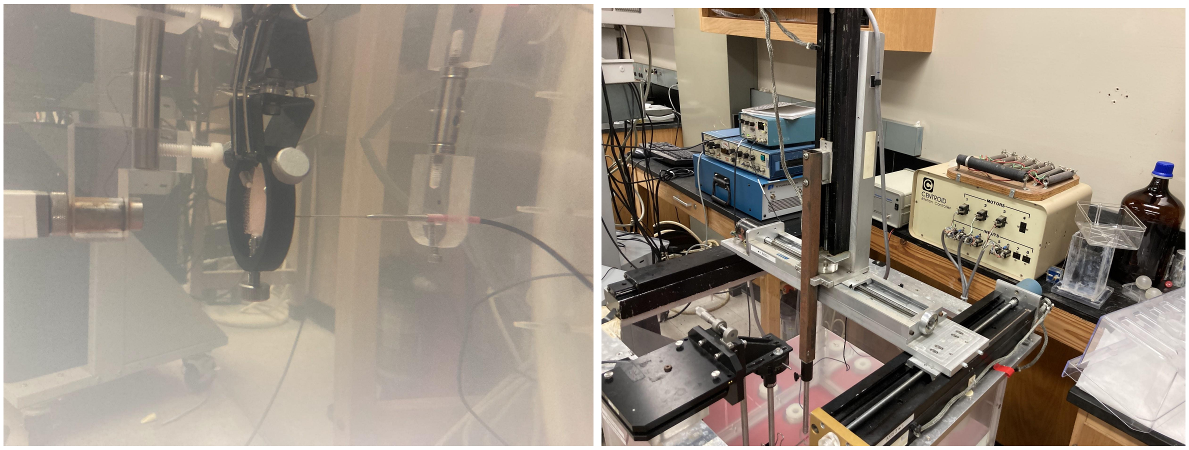

Figure 2.6: Left: the transducer on the far left, sample in the middle, and probe on the right. *Right:* The motion system that controls the probe position.

In this setup, samples were exposed to a smaller range of ultrasound, roughly 1-15 MHz with peak energy transmission occurring at 5 MHz. The transducer used has a traditional piezoelectric crystal element and a concave hemisphere surface with a focal point 2 inches (5.08 cm) from the transducer. Samples were placed 5.5 cm away from the transducer, close to the beginning of the far field. The measurement plane was set to 5 mm away from the back surface of the sample.

Chapter 3: Results

Section 3.1: Measurement Tank Results

Samples were placed in the measurement tank to identify the resonant frequencies of the samples. Resonances were identified from the attenuation curve produced from the spectra of the captured signals. The data downloaded to the computer was the average of 64 waveforms individually captured by the digital oscilloscope. The spectrum of the averaged signal was computed via fast Fourier transform (FFT). A MATLAB script controlled the acquisition and processing of the data. The spectrum was plotted with amplitude along the y axis and frequency along the x axis, and the waveform was plotted with amplitude in volts vs. time in microseconds. Before any samples were analyzed, an acquisition was taken of the water path that the ultrasonic beam travels to provide a baseline of the system response. The waterpath results can be seen in Figure 3.1, where both the averaged signal and the FFT are presented.

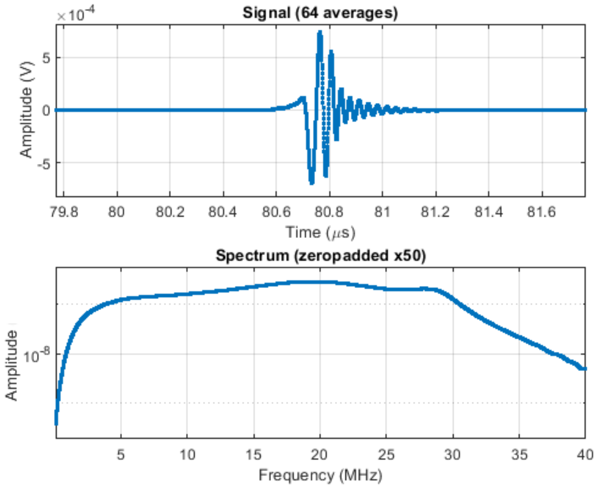

Figure 3.1: The averaged waveform for the waterpath acquisition is shown above, and the corresponding FFT spectrum is shown below. The pulse of the waveform has a regular shape, and the spectrum is mostly flat across the region of interest which allows variations due to scattering to be recognized.

Four types of samples were exposed to ultrasound in the measurement tank: orange scatterers (r = 98 µm), purple scatterers (r = 116 µm), red scatterers (r = 138 µm), and a mix of orange and purple scatterers. Further plotting is limited to below 15 MHz to highlight the unique dips of the frequency spectra. These dips are related to the scattering resonances. Data for the samples can be seen in Figures 3.2 - 3.5.

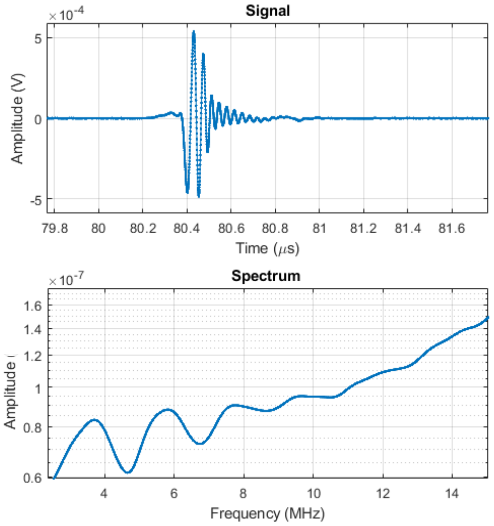

Figure 3.2: Signal and spectrum for the through sample acquisition, r = 98 µm

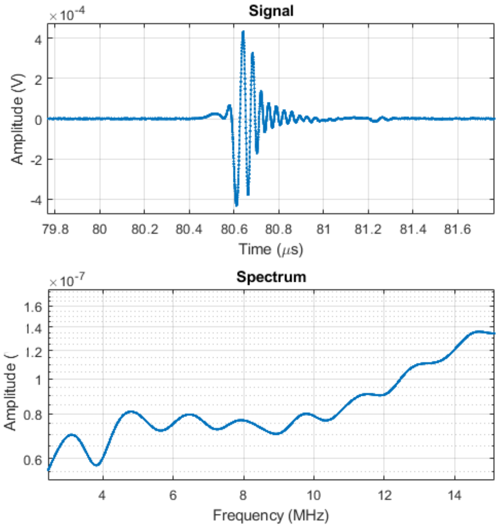

Figure 3.3: Signal and spectrum for the through sample acquisition, *r* = 116 µm

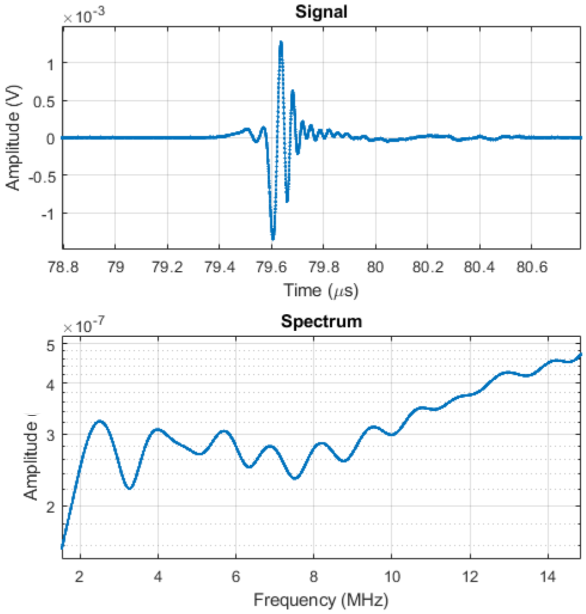

Figure 3.4: Signal and spectrum for the through sample acquisition, *r* = 138 µm

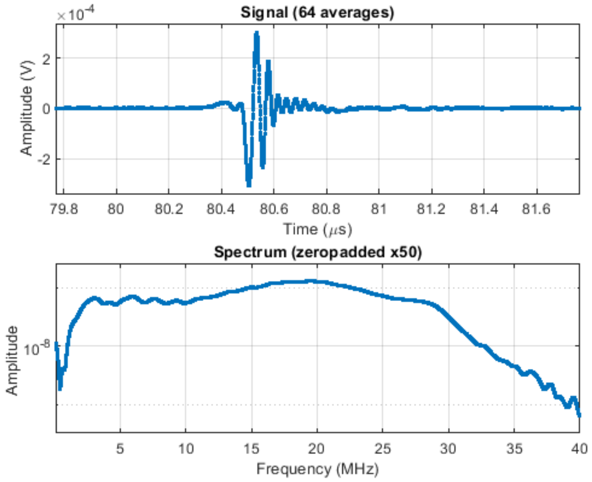

Figure 3.5: Signal and spectrum for the through sample acquisition, mixed 98 µm & 116 µm scatterers. Note the frequency axis was not scaled on this sample to show the relatively flat area of the spectrum from 15-30 MHz.

The data produced from interrogating a sample is a combination of the acoustic response from the system and the scatterers. To remove the response from the system and isolate the scattering response, further data processing is required. This will be discussed further in Chapter IV.

Section 3.2: Field Data

For samples placed in the field scanning tank, several waveforms are acquired at different locations on one side of the sample, producing a point by point pressure map over the scan plane. The captured waveforms are spectrally decomposed via FFT, and the resulting frequency spectra can be used to examine the spatial distribution of the frequency resolved field. The number of waveforms depends on the number of specified scan points, determined by the step size of the probe as it moves through the predetermined area. For example, a scan of a 15x15 mm area with a step size of 0.2 mm produces 7,569 individual waveforms. A plot of amplitude vs position was also created for each sample based on the peak to peak amplitude of the individual signals. Examples of these are shown in Figures 3.6 – 3.7 for the waterpath data.

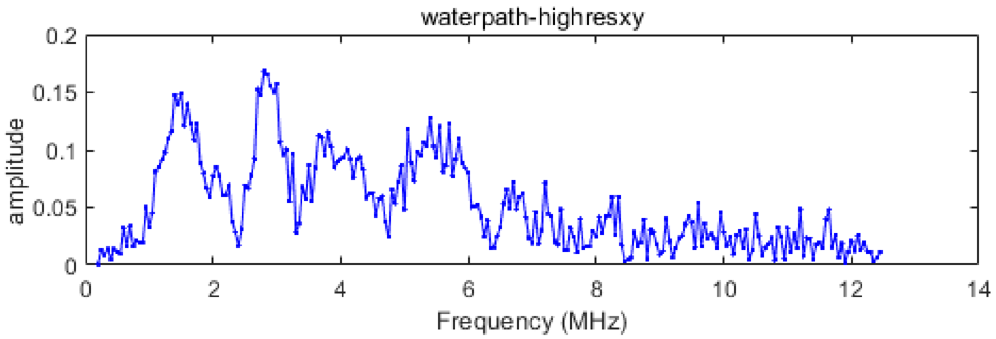

Figure 3.6: The frequency spectrum of the central point in the waterpath scan.

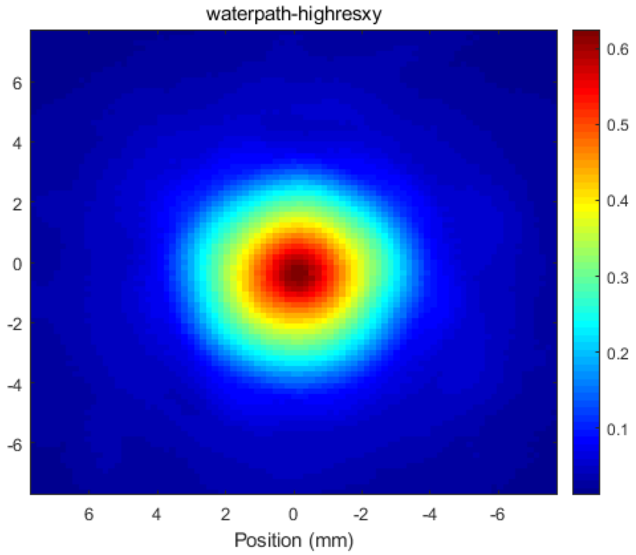

Figure 3.7: Pressure vs position of the water path scan. The color represents the amplitude.

The pressure data was also plotted in a surface format. The image and surface plots of the samples are shown in the following figures:

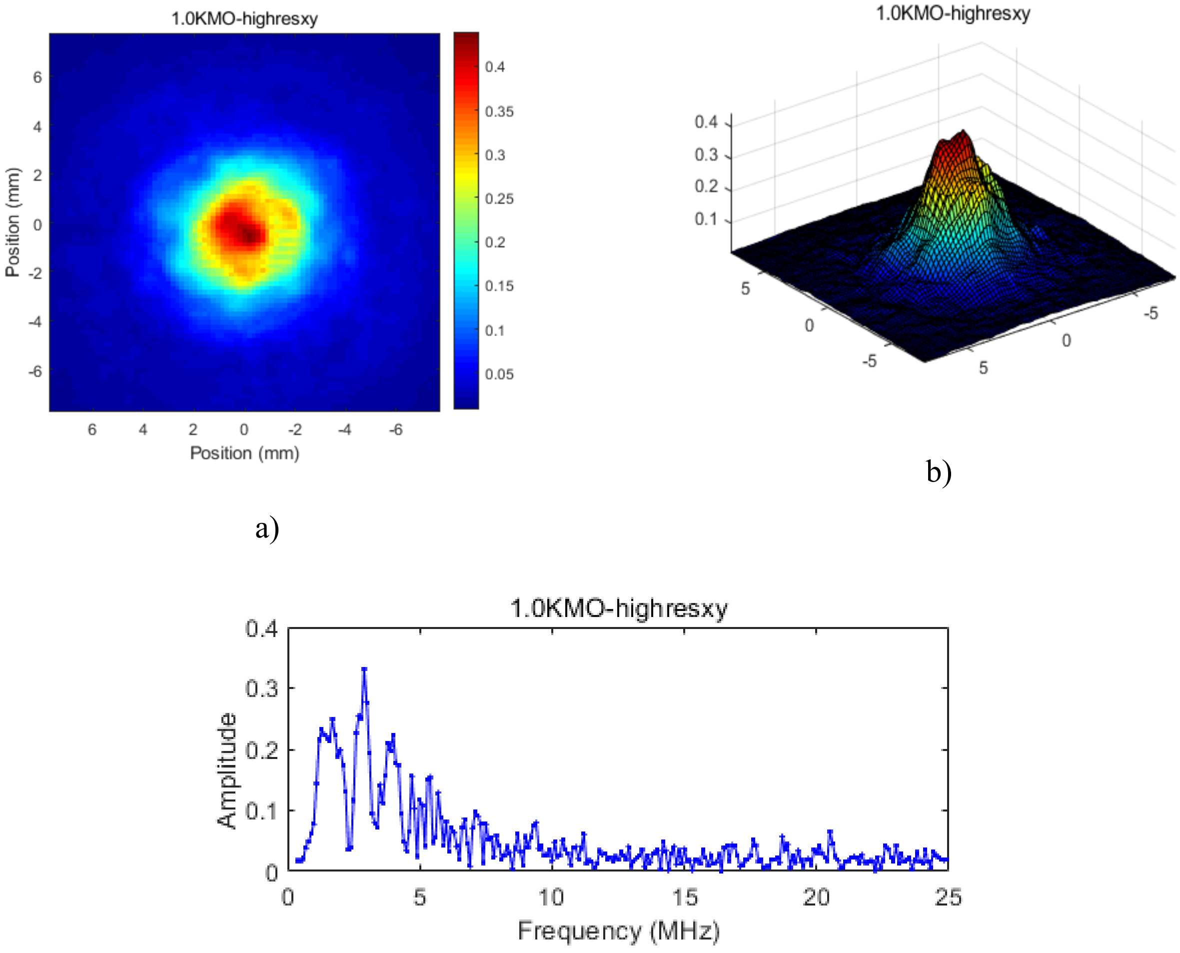

a)

b)

c)

Figure 3.8: a) Pressure vs position, amplitude is represented by color, for r = 98 µm. b) the surface plot of pressure vs position for r = 98 µm . c) The frequency spectrum of the central point in the scan.

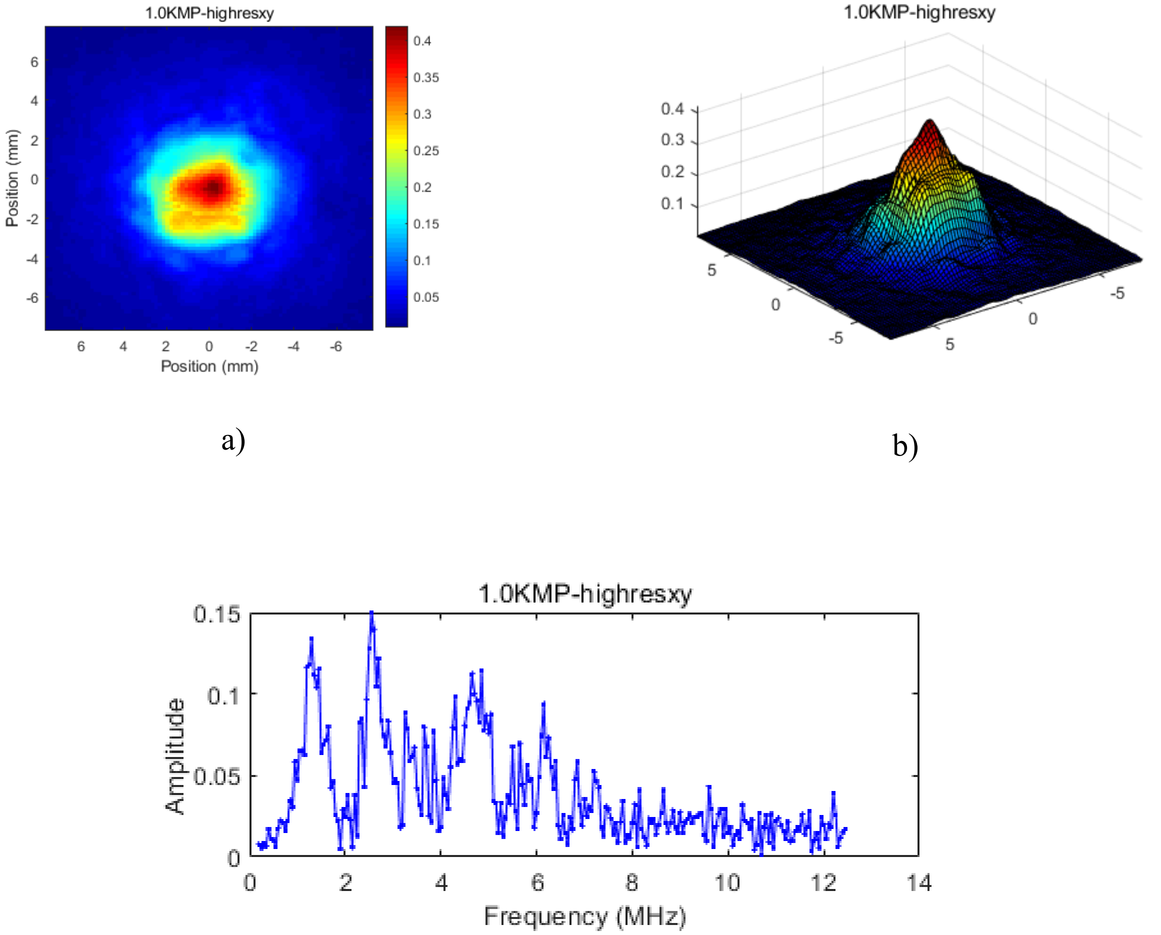

a)

b)

c)

Figure 3.9: a) Pressure vs position, amplitude is represented by color, for r = 116 µm. b) the surface plot of pressure vs position for r = 116 µm . c) The frequency spectrum of the central point in the scan.

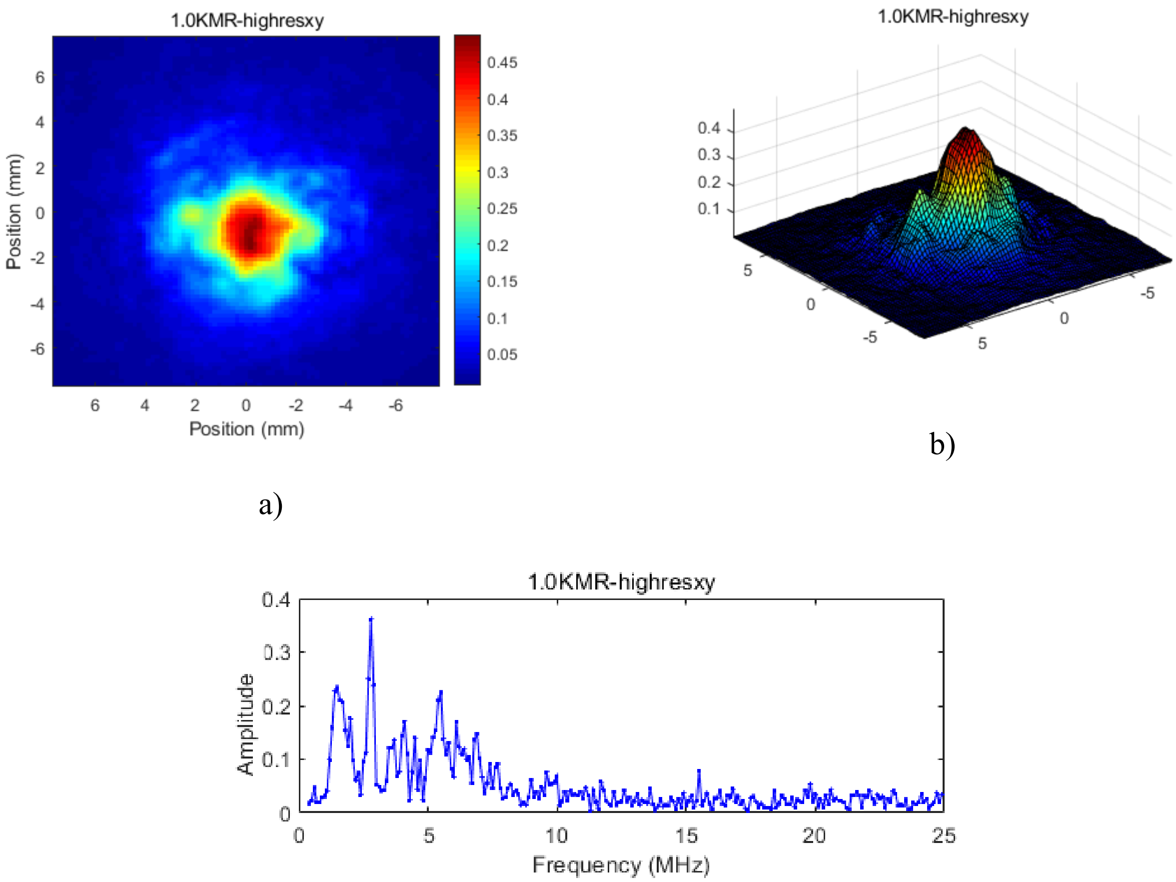

a)

b)

c)

Figure 3.10: a) Pressure vs position, amplitude is represented by color, for *r* = 138 µm. b) the surface plot of pressure vs position for *r* = 138 µm . c) The frequency spectrum of the central point in the scan.

Chapter 4: Analysis

Section 4.1: Acoustic Measurement Analysis

Resonant frequencies were not identified directly from the frequency spectrum produced from the FFT of the recorded waveform. Dips in the frequency spectrum are indicative of resonances. However the sample data includes acoustic responses from both the scatterers in the sample and the acquisition system itself. The process to separate these responses is accomplished in the frequency domain. The waveform recorded from the sample can be modeled using Equation 4.1.

$$q(t) = \int_{-\infty}^{\infty} w(t')p(t - t')dt' \qquad (4.1)$$

$q(t)$ is the waveform recorded from a sample, $f(t')$ is the impulse from the incoming ultrasound, and $p(t - t')$ is the natural transfer function of the scatterers. The Fourier transform of Eq. 4.1 results in the separable Equation 4.2, which can be manipulated to isolate the spectrum of the transfer function.

$$Q(\omega) = W(\omega)P(\omega) \qquad (4.2.a)$$

$$P(\omega) = \frac{Q(\omega)}{W(\omega)} \qquad (4.2.b)$$

$Q(\omega)$ is the recorded sample spectrum, $W(\omega)$ is the spectrum of the water path data, and $P(\omega)$ is the spectrum of the transfer function. The transfer function representing the acoustic response of the scatterers is separated from recorded data by dividing the sample spectrum by the water path spectrum, which represents the response of the acquisition system. The transfer functions produced from this method are plotted as transmitted amplitude vs. frequency. The spectrum of the transfer function can be modeled using Equation 4.3.

$$P(\omega) = \overline{P_o} e^{-\alpha x} e^{-\frac{i\omega}{c}x} \qquad (4.3)$$

$\overline{P_o}$ is the maximum response amplitude, α is the attenuation coefficient, x is the thickness of the sample, ω is the angular frequency, and c is the speed of sound in the scatterer. Manipulation of Eq. 4.3 leads to the set of proportions, Equations 4.4 – 4.6.

$$P(\omega) \propto e^{-\alpha x} \qquad (4.4)$$

$$\frac{Q(\omega)}{F(\omega)} \propto e^{-\alpha x} \qquad (4.5)$$

$$-\ln\left(\frac{Q(\omega)}{F(\omega)}\right) \propto \alpha x \qquad (4.6)$$

The left hand side of Eq. 4.6 can be used to create a graph that represents the attenuation of the scatterers, and peaks in these graphs correspond directly to the resonant frequencies. The transfer functions and attenuation curves for the various sized scatterers can be seen in the following figures.

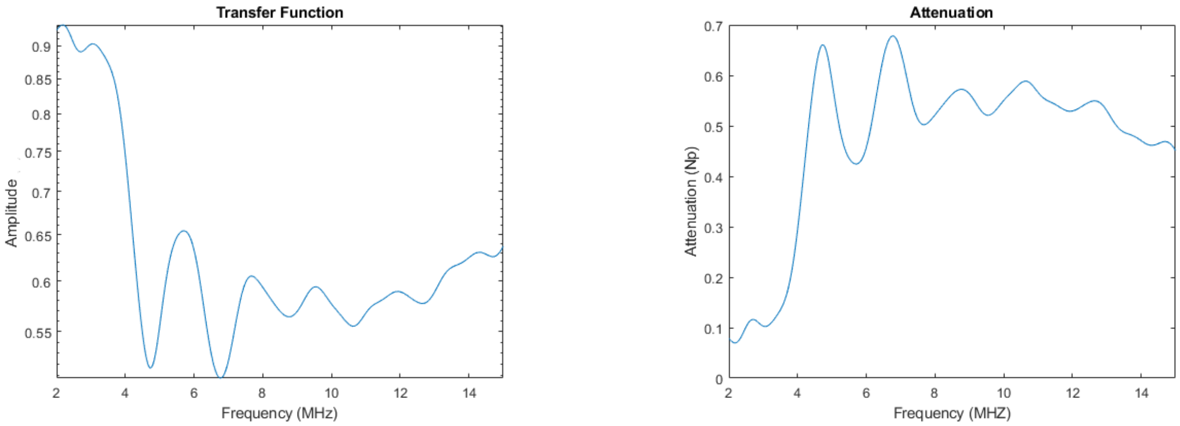

a) b)

Figure 4.1: a) Transfer function of the r = 98μm scatterers. b) Attenuation curve of the r = 98μm scatterers. Frequencies associated with the peaks of the attenuation curve are 4.7, 6.7, 8.7, 10.7, 12.7 MHz

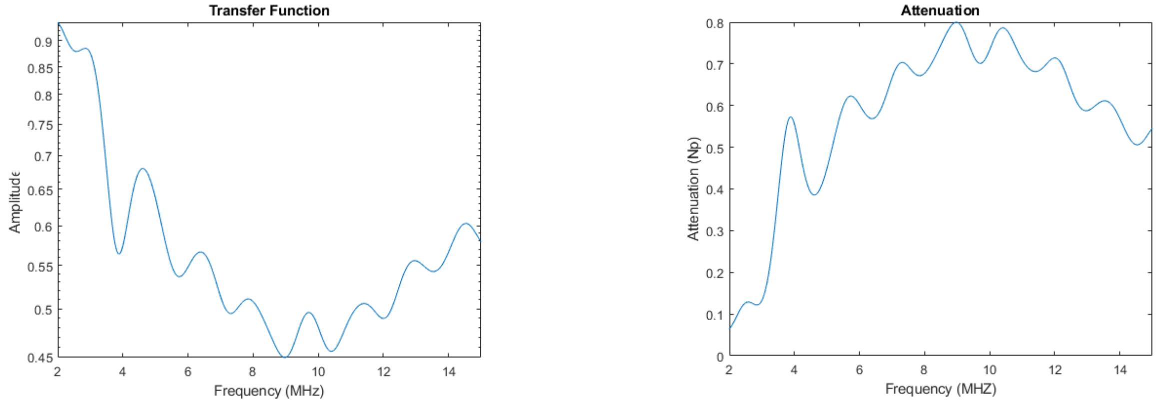

a) b)

Figure 4.2: a) Transfer function of the *r* = 116 μm scatterers. b) Attenuation curve of the *r* = 116 μm scatterers. Frequencies associated with the peaks of the attenuation curve are 3.9, 5.7, 7.3, 9.0, 10.4, 12.0, and 13.6 MHz

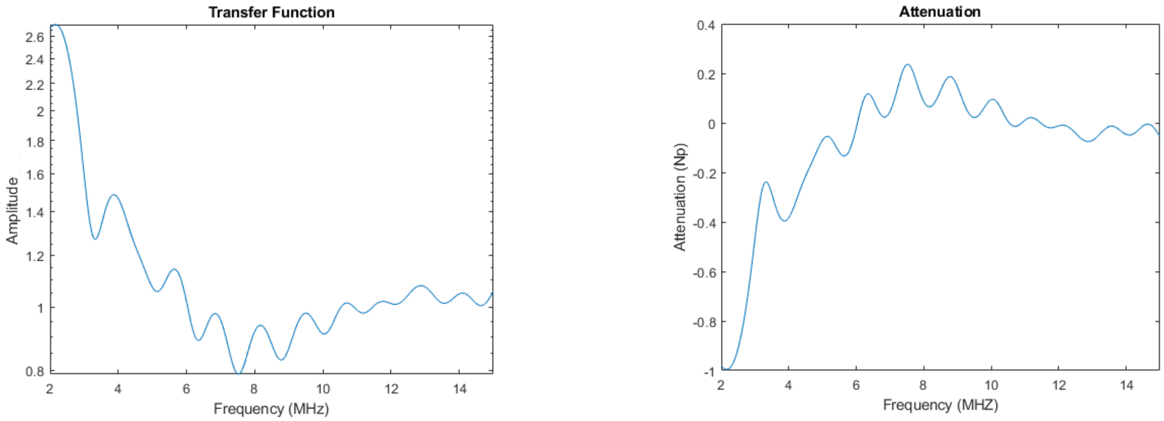

a) b)

Figure 4.3: a) Transfer function of the $r = 138$ µm scatterers. b) Attenuation curve of the $r = 138$ µm scatterers. Frequencies associated with the peaks of the attenuation curve are 3.3, 5.1, 6.4, 7.5, 8.8, 10.0, 11.2, 12.1, 13.5, and 14.6 MHz

The attenuation curves provide the resonant frequencies used to analyze the 2D pressure field data. Scattering orders were determined by taking the product of the wave vector at each frequency and the circumference and comparing each product to the peaks in Fig. 1.4. It was determined that the first observed resonant mode of each scatterer type corresponded to the second scattering mode. Following modes were assigned from this starting point. It was found that the first resonant frequency for each scattering type had an average ka value of 1.2, which corresponds to the second scattering order. Table 4.1 lists the scattering order and frequencies of the major resonant modes identified from the attenuation curves.

Scattering order	r = 98 µm (MHz)	r = 116 µm (MHz)	r = 138 µm (MHz)
2	4.7	3.9	3.3
3	6.7	5.7	5.1
4	8.7	7.3	6.4
5	10.7	9.0	7.5
6	12.7	10.4	8.8
7		12.0	10.0
8		13.6	11.1
9			12.1
10			13.5

Table 4.1: Frequencies of the resonant modes identified for each scatterer type. The scattering order was determined using Fig. 1.4.

Eight potential pairs of scattering modes were identified from this list based on frequency proximity and scattering order. A particular scattering mode will be denoted using R_r^n, where n is the scattering order and r is the radius of the scatterer. The potential pairs are $[R_{98}^{4}\ R_{138}^{5}]$, $[R_{98}^{5}\ R_{138}^{6}]$, $[R_{98}^{6}\ R_{116}^{7}]$, $[R_{116}^{6}\ R_{138}^{7}]$, $[R_{98}^{7}\ R_{116}^{8}]$, $[R_{98}^{7}\ R_{138}^{10}]$, $[R_{116}^{7}\ R_{138}^{8}]$, $[R_{116}^{8}\ R_{138}^{9}]$. (Average frequencies in order, MHz: 4.9, 6.6, 8.9, 7.4, 10.6, 10.9, 8.9, 10.2) Linear combinations of the attenuation curves are plotted to see if the potential overlapping frequencies will overlap effectively, and those plots are presented in the following figures.

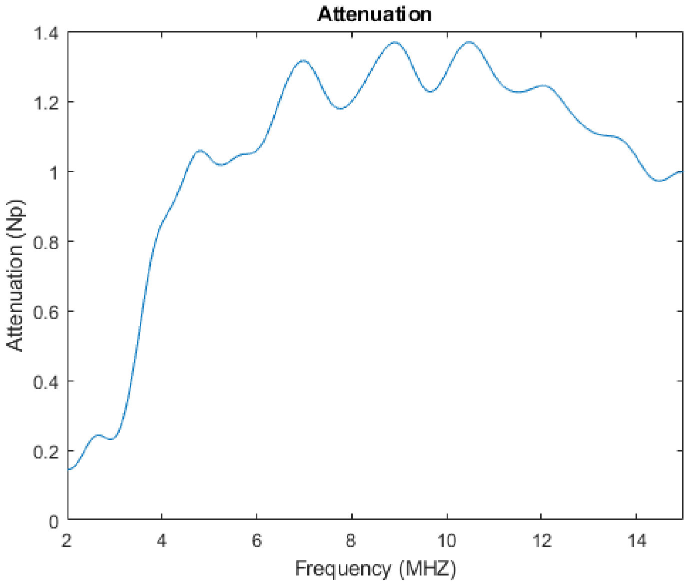

Figure 4.4: The linear combination of *r* = 98 µm and *r* = 116 µm. The three sharpest peaks correspond to frequencies 6.9, 8.9, and 10.5 MHz. The 6.9 MHz peak is likely the distorted second harmonic frequency of the smaller scatter (6.8 MHz), while the 8,9 and 10.5 MHz peaks line up with the predicted overlapping modes.

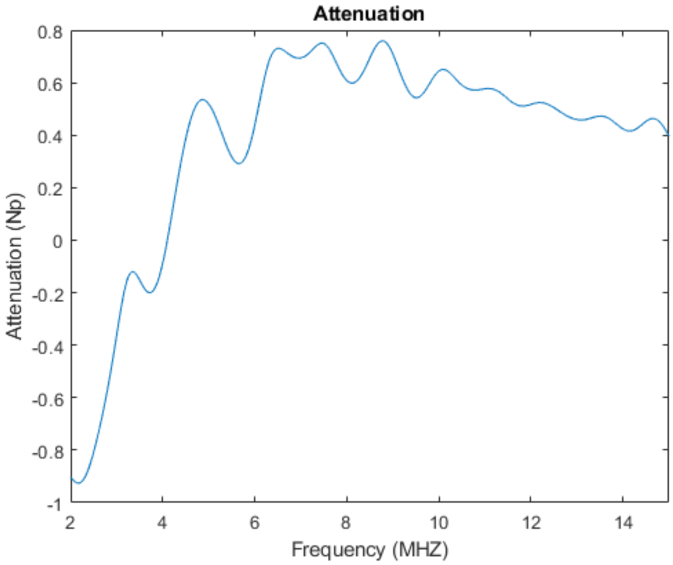

Figure 4.5: The combination of the *r* = 98 µm and *r* = 138 µm attenuation curves. The first peak at 3.3 MHz corresponds to the first resonant frequency of the large scatterer, and the second peak at 4.8 MHz is close to a predicted overlap. There are two peaks around the area where the second overlap was predicted, and the peak around 8.7 corresponds to overlapping modes of the same type. The peak at 10.1 MHz is likely an overlap of alternating orders

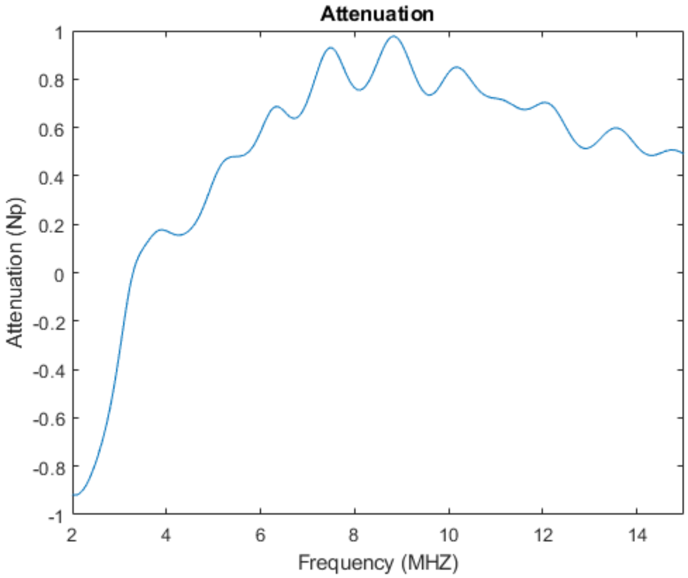

Figure 4.6: The linear combination of $r = 116$ µm and $r = 138$ µm sized scatterers. The three largest peaks at 7.6, 8.9 and 10.2 MHz correspond to predicted overlapping modes, and the other peaks correspond to either the characteristic frequencies from either scatterer size, or the overlap from the same type of resonant mode.

Section 4.2: 2D Pressure Field Analysis

The process for separating the transfer function from the recorded sample signal is necessary to extract usable data from the 2D pressure field scans. This process was scripted using MATLAB to produce a frequency spectrum for each recorded waveform in the scan plane. The 2D transfer function can be plotted as a two dimensional pressure distribution relative to frequency, and the pressure distribution at the resonant frequencies determined from the acoustic measurement data are plotted in the following figures

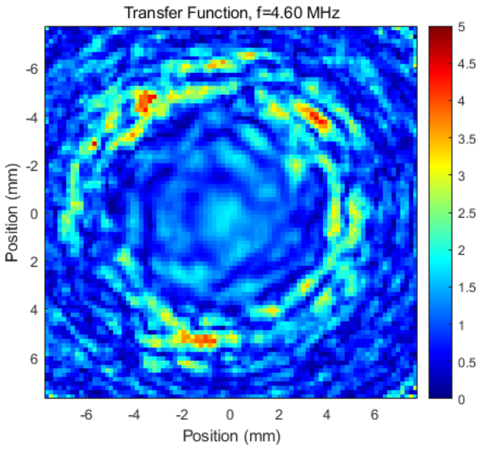

Figure 4.7: The relative pressure distribution at the first resonance frequency for $r = 98$ µm (4.6 MHz)

-

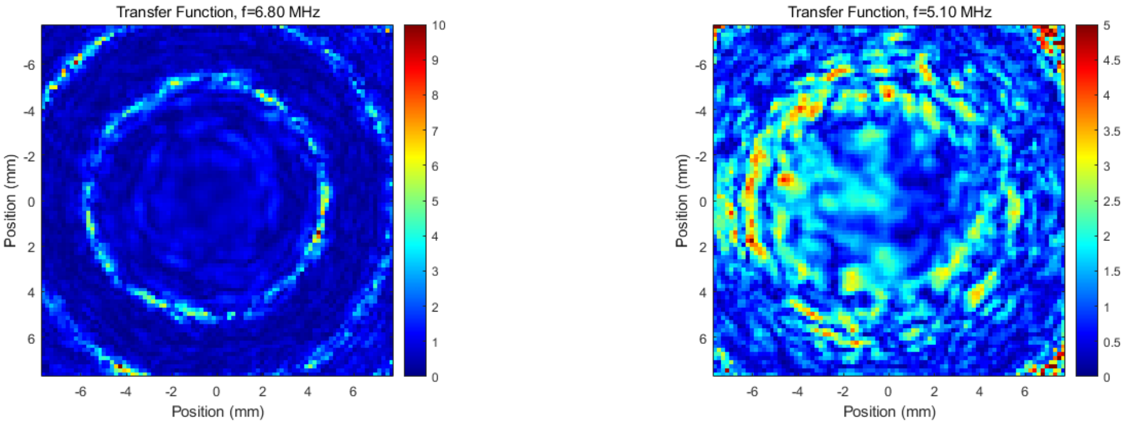

a) b)

Figure 4.8: The pressure distribution of the second resonance frequency for a) $r = 98$ µm (6.8 MHz), b) $r = 138$ µm (5.1 MHz)

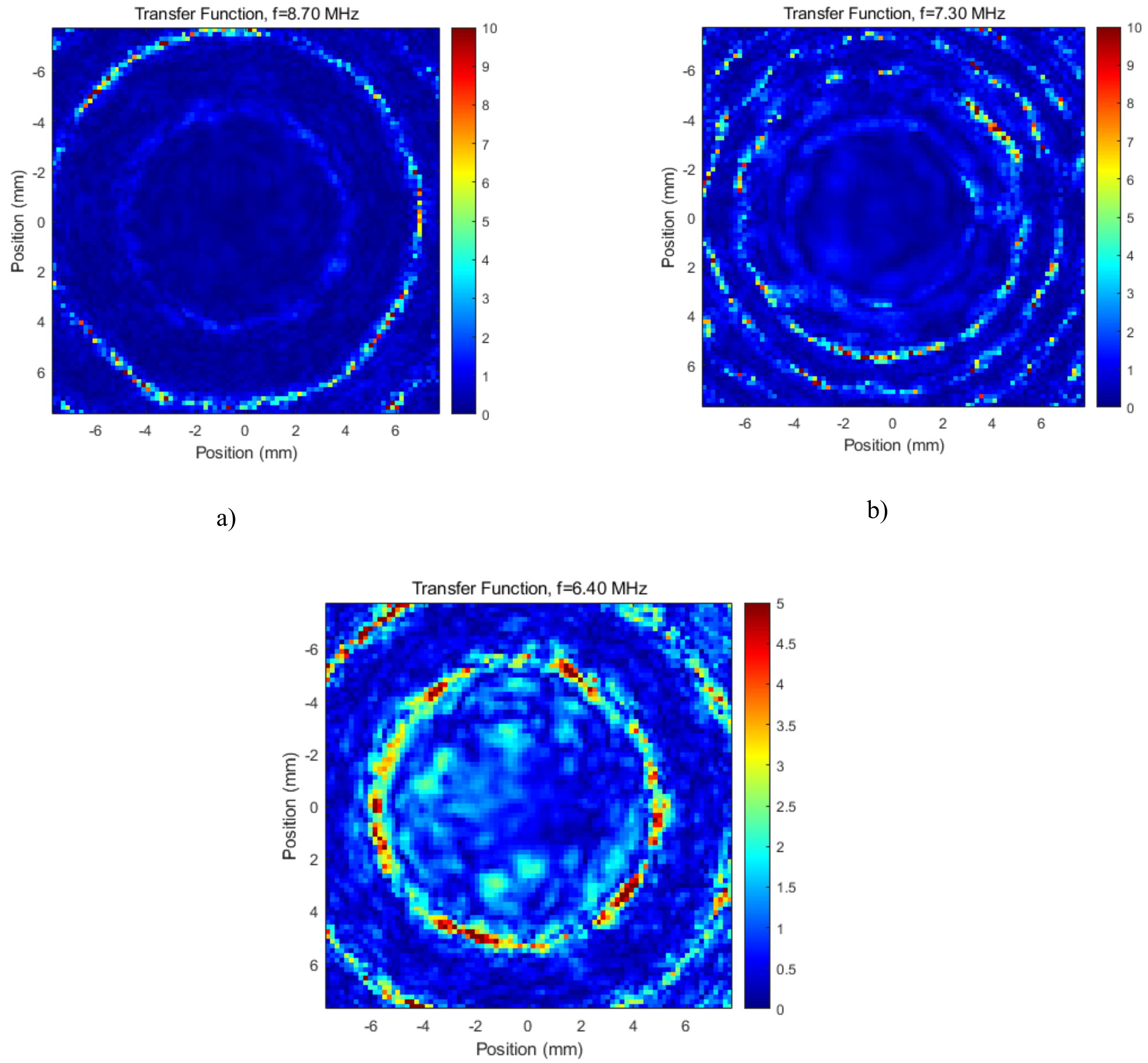

a)

b)

c)

Figure 4.9: The pressure distribution of the third resonance frequency for a) r = 98 μm (8.7 MHz), b) r = 116 μm (7.3 MHz), c) r = 138 μm (6.4 MHz)

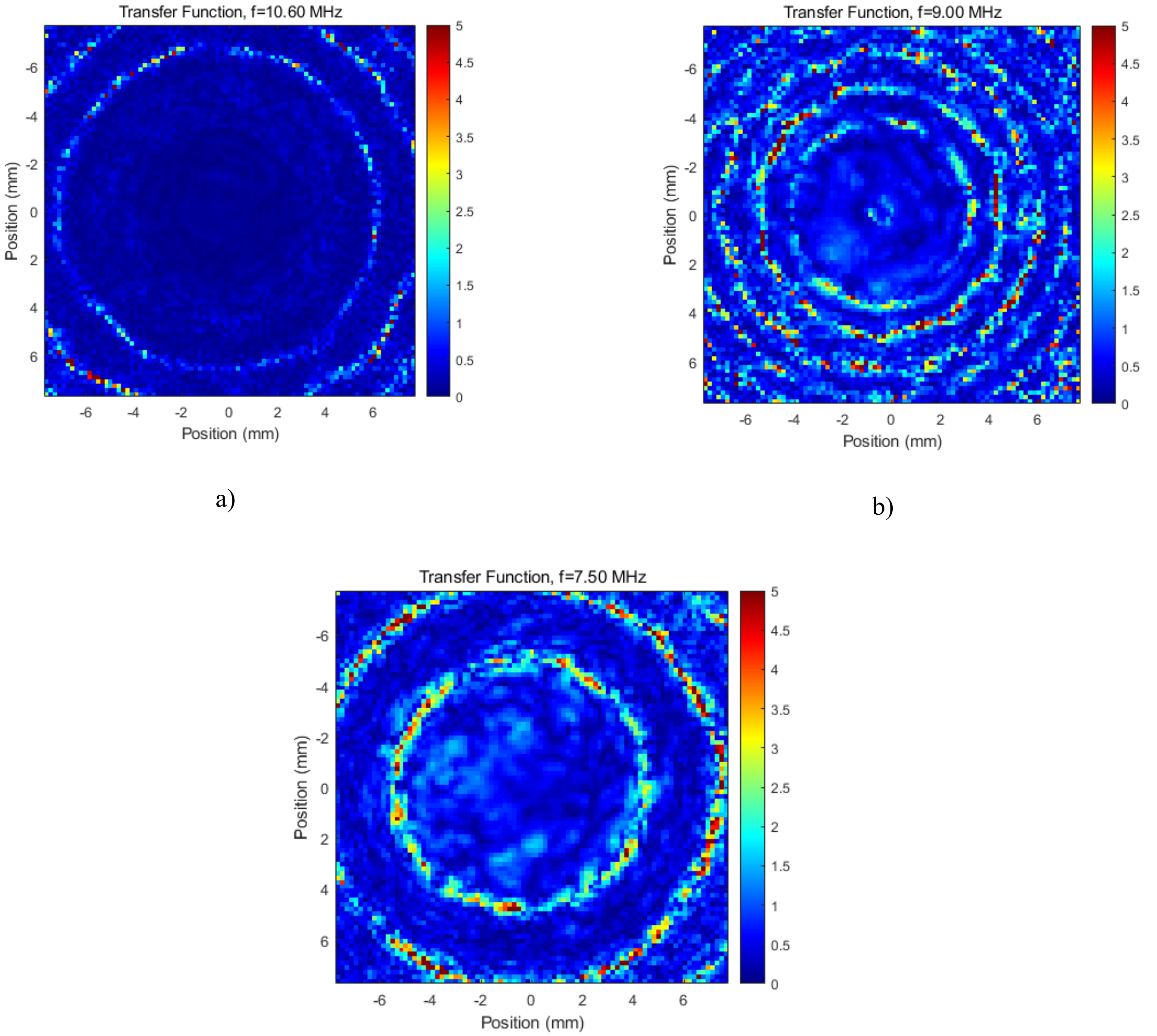

a)

b)

Figure 4.10: The pressure distribution of the fourth resonance frequency for a) r = 98 µm (10.6 MHz), b) r = 116 µm (9.0 MHz), c) r = 138 µm (7.5 MHz)

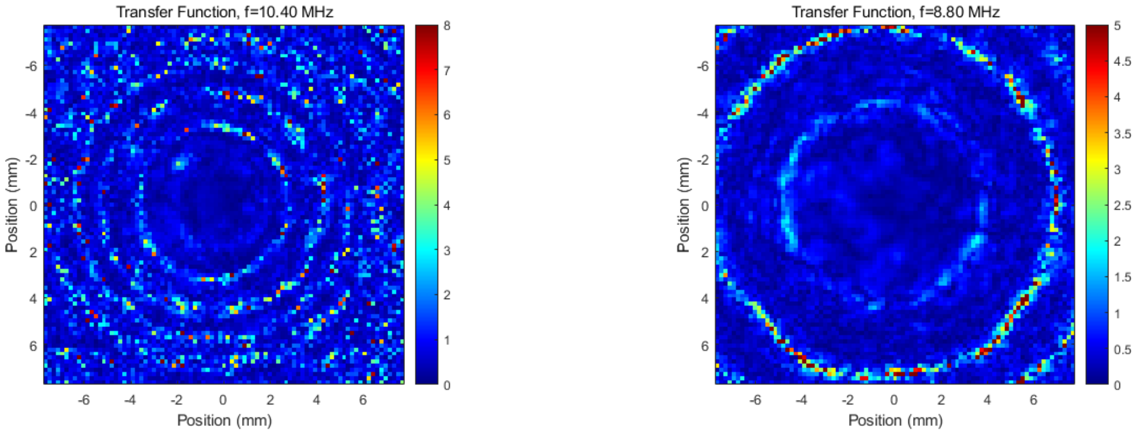

a)

b)

Figure 4.11: The pressure distribution of the fifth resonance frequency for a) r = 116 µm (10.4 MHz), b) r = 138 µm (8.8 MHz)

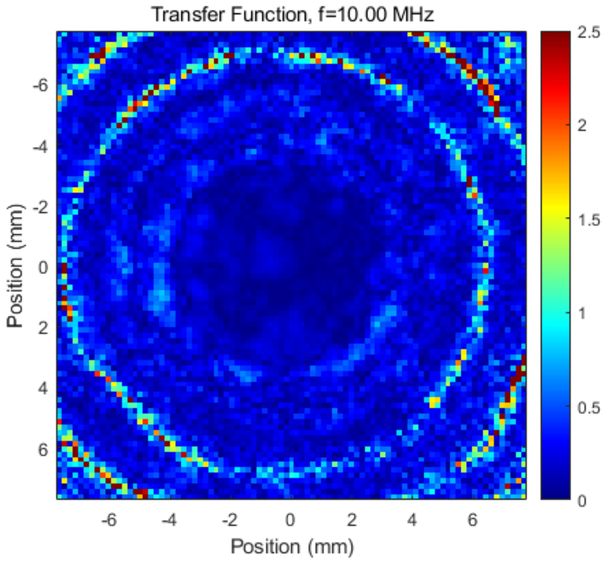

Figure 4.12: The pressure distribution for the sixth resonance frequency for r = 138 µm (10.0 MHz)

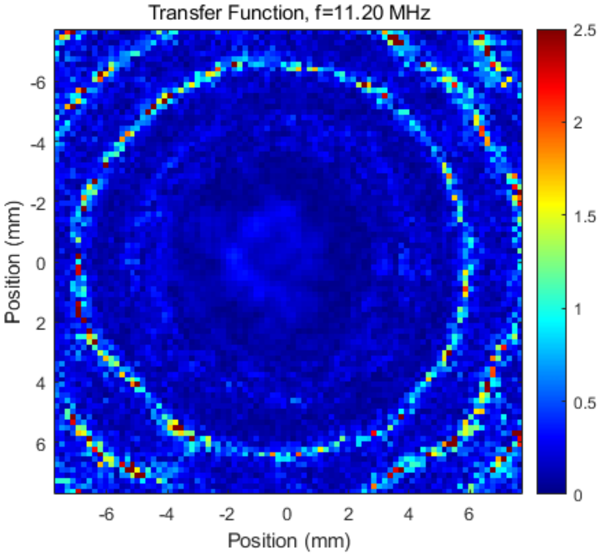

Figure 4.13: The pressure distribution of the seventh resonance frequency for r = 138 µm (11.2 MHz)

Anomalous bands can be seen in the field projections for the r = 116 µm scatterers. These bands are considered anomalous because they are likely results of diffraction patterns in the water path data that create minimized bands, which appear as areas of high pressure after the transfer function has been separated from the recorded data.

Chapter V: Conclusions

A method for creating a gelatin matrix that could hold a random array of microspheres was developed, using gelatin as the major component. Samples could be produced within 20 minutes, and measurements could be made almost immediately after production. Acoustic measurements were performed for the purpose of determining resonant frequencies of the scatterer samples. The 1.0 ks/ml samples produced strong responses in the range of 1-15 MHz, and weak responses in the range above 15 MHz to 35 MHz. By focusing on the range with the strongest response, several resonant frequencies were identified for each type of microsphere studied. The mixed scatterers were abandoned after these initial trials due to the additional steps in separating the resonant modes of the two scatterers. The effect of adding two types of scatterers is a linear one; the observed spectrum of the mixed sample is the same as the superposition of the two individual scattering spectra. With individual data on the three sizes of scatterers, linear combinations of the attenuation curves were created to determine whether the proposed pairs of resonant frequencies favorably overlap. Of the proposed pairs, only $[R_{98}^{5}\ R_{138}^{6}]$ did not agree with the linear combinations of the attenuation curve. This is likely due to the presence of R_{98}^{5} being evenly spaced between R_{138}^{6} and R_{138}^{7} in frequency. The presence of strong peaks on the combined attenuation curves confirms that the selected resonance frequencies are fit for further analysis. The 2D pressure field data is inconclusive for several reasons. While the scattering order could be recognized from the transfer function when compared with theory, it could not be resolved whether the fields will actually interact favorably with each other. Linear combinations of spectral distributions were attempted, but issues in scan array indexing have prevented the $r = 116$ μm data set from being accurately combined with the other data sets. Furthermore, there are strong pressure bands in the spectral distribution plots that do not match any projected angular distributions for the appropriate modes. Attempting to resolve the data in terms of magnitude, phase , and real and imaginary parts did not help with resolving the source of the anomalous bands. These bands are likely artifacts of the diffraction pattern created by the ultrasound beam traveling through the waterpath. While microspheres do indeed support the range and types of resonant modes necessary to create acoustic metamaterials, further research is needed to determine if these modes will superimpose favorably to produce the desired negative properties.

Bibliography

1. Mohammad Mahdi. (2013). *Integrated Circuit Design for Flip-Chip Bonded Capacitive Micromachined Ultrasonic Transducers* (Masters Thesis) Middle East Technical University, Ankara, Turkery. retrieved from https://researchgate.net
2. Yun Lai, Ying Wu, Ping Sheng and Zhao-Qing Zhang, “Hybrid elastic solids”, Nature Materials10, 620-624 (2011) https://doi.org/10.1038/NMAT3043
3. Guancong Ma, Ping Sheng, “Acoustic metamaterials: from local resonances to broad horizons”, Science Advances 2, 2 (2016) https://doi.org/10.1126/sciadv.1501595
4. Jensen Li, Xinhua Wen, and Ping Sheng, "Acoustic metamaterials", Journal of Applied Physics 129, 171103 (2021) https://doi.org/10.1063/5.0046878
5. Michael R. Haberman *and* Matthew D. Guild, "Acoustic metamaterials", Physics Today 69, 42-48 (2016) https://doi.org/10.1063/PT.3.3198
6. Joel Mobley (1998) *Measurements and Predictions of the Phase Velocity and Attenuation Coefficient in Suspensions of Elastic Microspheres* (Doctoral dissertation) Washington University, St. Louis, USA.
7. Joel Mobley, Jon N. Marsh, Christopher S. Hall, Michael S. Hughes, Gary H. Brandenburger, and James G. Miller, "Broadband measurements of phase velocity in Albunex® suspensions", The Journal of the Acoustical Society of America 103, 2145-2153 (1998) https://doi.org/10.1121/1.421360
8. Christopher S. Hall, Jon N. Marsh, Michael S. Hughes, Joel Mobley, Kirk D. Wallace, James G. Miller, and Gary H. Brandenburger, "Broadband measurements of the attenuation coefficient and backscatter coefficient for suspensions: A potential calibration tool", The Journal of the Acoustical Society of America 101, 1162-1171 (1997) https://doi.org/10.1121/1.418020
9. James J. Faran Jr. , "Sound Scattering by Solid Cylinders and Spheres", The Journal of the Acoustical Society of America 23, 405-418 (1951) https://doi.org/10.1121/1.1906780

VITA

ALEXANDER DENETTE

---

145 Hill Drive NCPA, University, MS, 38677 | aodenett@go.olemiss.edu

EDUCATION

MS, Physics, University of Mississippi, August 2022

Concentration: Ultrasonic Acoustics

Thesis: Investigating the Acoustic Properties of Polymer Microspheres suspended in Gelatin

BS, Chemistry, University of Mississippi, August 2019

Minor: Mathematics

Research Focus: Computational Chemistry

BA, Physics, University of Mississippi, August 2019

TEACHING EXPERIENCE

- Graduate Teaching Assistant, University of Mississippi- Freshman Physics Lab, Remote Lecture Assistance, Grading (2019-2021)

- Mathematics Tutor, University of Mississippi- College Algebra, Calculus I-IV, Business Calculus, (2016-2018)
- Private Tutor, Self Employed - Introductory Chemistry, Organic Chemistry, Introductory Physics (2016-2020)

RESEARCH EXPERIENCE

- Graduate Research Assistant, Ultrasonics Group, National Center for Physical Acoustics, University of Mississippi (2022)
    - Thesis research into acoustic properties of microspheres exposed to ultrasonic pulses.
- Undergraduate Research Assistant, Tschumper Research Group, Department of Chemistry and Biochemistry, University of Mississippi (2016-2019)
    - Research into hydrogen bonding and computational efficiency for *ab initio* quantum mechanical modeling of simple chemical systems.